Deutscher Luft- und Raumfahrtkongress 2009
DocumentID: 121165

EXTENDING THE DESIGN PARAMETER SPACE OF A HIGHLY LOADED HIGH PRESSURE COMPRESSOR STATOR THROUGH APPLICATION OF NON-AXISYMMETRIC ENDWALL CONTOURING

F. HEINICHEN*, V. GÜMMER*, H.-P. SCHIFFER**

*Rolls-Royce Deutschland, Eschenweg 11, 15827 Blankenfelde-Mahlow
**TU Darmstadt, Petersenstrasse 30, 64287 Darmstadt

ABSTRACT

The application of non-axisymmetric contours to the endwalls of axial turbine blade rows has been successfully used for a number of years. The potential of this technology to also improve the performance of high pressure compressors is the focus of a number of recently published investigations. The results seem to indicate that a significant improvement of the relevant flow parameters can only be achieved under specific conditions. The study presented in this paper uses a highly loaded stator blade row to numerically verify the hypothesis that the main condition, which determines whether the application of non-axisymmetric endwall contouring has a significant impact on the flow, is the presence of an extensive reverse flow area close to the endwalls. In order to assess this, non-axisymmetric endwall contours were applied to a baseline stator at the hub and casing with a semi-automated optimisation process. In a second step, the number of blades was reduced by approximately 18 %, which resulted in the development of a pronounced flow separation zone close to the stator casing. As a last step, non-axisymmetric endwalls were applied at hub and casing of this new stator. The results of steady 3D viscous flow calculations were compared for the four resulting configurations at design speed conditions. While application of non-axisymmetric endwalls to the baseline stator only resulted in an increase in polytropic efficiency of about 0.05 % at design point conditions, an increase of 1.2 % was observed for the stator with reduced number of blades. The results demonstrate that the potential of non-axisymmetric endwall contouring in high-pressure compressors to improve the design in terms of cost, weight and aerodynamic performance can be best exploited by making use of the increased design parameter space rather than simply applying the method to a given design.

1 INTRODUCTION

Until very recently, non-axisymmetric endwall contouring was a turbomachinery technology feature that could only be found in axial turbines. However, while there is no obvious reason why using non-axisymmetric hub or casing geometries should not help to improve the aerodynamic behaviour of axial compressors as well, only few attempts have been reported to do so. Even though similarities exist between compressors and turbines in terms of secondary flow features, their aerodynamics are fundamentally different. This complicates any attempt to translate the basic parameters of successful non-axisymmetric turbine endwall contours into the compressor environment and raises questions about the underlying mechanisms that are to be exploited by this feature.

While some studies have been performed with axisymmetric or non-axisymmetric contours on high-pressure compressor rotors [1], [2], [3], non-axisymmetric endwalls seemed to lead to much higher performance improvements when applied to stator blade rows or struts [4], [5], [6]. A review of the literature currently available seems to indicate that of non-axisymmetric endwall contours can be particularly well applied to stators that exhibit a significant zone of reverse flow close to the endwall that is to be contoured, spawning speculations that the contours have a similar potential to suppress stator corner separation as conventional three-dimensional de-

sign methods like aerofoil lean and sweep [7], [8].
The numerical study presented in this paper aims to investigate the stall-suppressing potential of non-axisymmetric endwalls beyond the level of 3D aerofoil stacking. A highly loaded stator row, that does not show significant separation at design point conditions was loaded even further by reducing the number of blades. The resulting reverse flow area near the casing could not be suppressed by 3D aeroil stacking alone. The corner stall could only be reduced in size after application of non-axisymmetric endwalls to the stator. By analysing the detailed flow field at design point for both the stator axisymmetric and non-axisymmetric endwalls and by relating the findings to the impact that the endwall contouring method has on the baseline configuration , it is confirmed that suppression of corner stall is the main flow feature that can be controlled by non-axisymmetric endwall contours. Furthermore, it is demonstrated that the additional stall-suppressing potential of this feature can be used together with conventional 3-D aerodynamic design methods to expand the design parameter space, in this case the range of feasible stator blade numbers.

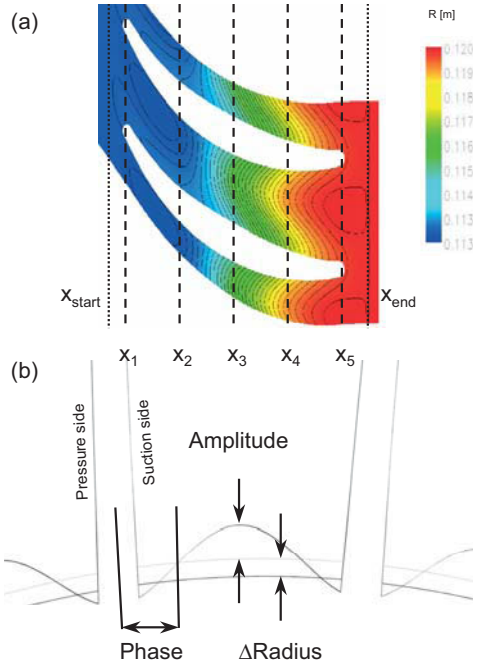

FIG 1. Sketch outlining the axial (a) and circumferential (b) parametrisation of the non-axisymmetric endwall contour.

2 METHODS

2.1 CFD System

The results of all steady calculations presented in this paper were generated with the Rolls-Royce in-house CFD suite Hydra. It consists of meshing and preprocessing tools, the actual flow solver and a number of different postprocessors. The initial multiblock structured mesh is generated by the parametric meshing and design tool PADRAM [9]. The software enables rapid meshing of aerofoil and annulus geometry as well as secondary geometry features like fillets, VSV part clearances, rotor running gaps, bleed off-takes and shrouds. The mesh features a hybrid O-H topology, with several layers of O-mesh around the aerofoil and H-grid cells in the blade passage, near the periodic boundaries and in the inlet and outlet sections. The mesh is clustered towards the endwalls as well as the blade surface. The wall distance of the first cell was set to result in a level of y^+ of 20 or lower on all solid surfaces, which was considered sufficient for the employed Spalart-Almaras turbulence model with wall functions.
The flow solver itself has an edge-based data structure and is capable of running unstructured, multigrid steady or unsteady CFD calculations with parallel processing. Each blade row of the compressor is modelled as a separate computational domain. Circumferentially averaged flow parameters pressure, temperature and the components of the velocity vector are exchanged between the individual blade rows via mixing planes. The compressor inlet boundary conditions are defined as circumferentially constant radial distributions of total pressure and temperature, whirl and radial flow angles as well as turbulence level. At compressor exit, a radial equilibrium boundary conditions is prescribed with a single value of static pressure close to the inner annulus. Calculations are run at constant rotational speed and different values of exit static pressure. The highest pressure at which a converged solution can be obtained is considered the numerical stall point. This condition was used as an estimate for compressor stability when comparing the different variants presented in this investigation.

2.2 Definition of non-axisymmetric endwalls

The non-axisymmetric endwall contours are generated by PADRAM during the meshing process. The contour is defined as circumferential harmonic perturbations of the original endwall contour at prescribed axial locations. Perturbations of different order and amplitude can be superimposed at the same axial position. The perturbation starts on the camber line of the aerofoil endwall section and the phase length is equal to one blade pitch at the axial location under consideration. Furthermore, two additional axial positions are defined that mark the beginning and end points of the contoured endwall.

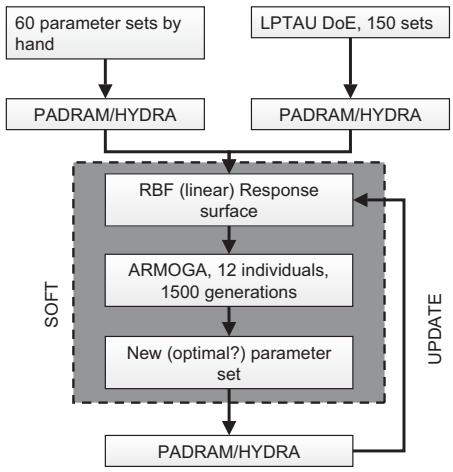

FIG 2. Semi-automated design procedure for non-axisymmetric endwalls that was developed for this study.

For the current investigation, non-axisymmetric endwalls were designed on both the hub and casing endwalls of the stator. The contour range was set to be equal to the axial length of the stator platform. Circumferential perturbations were defined at five equally spaced axial positions. The first position was at the leading and the last one coincided with the trailing edge of the aerofoil section, as shown in FIG 1 (a). At each axial location, harmonics of zero, first and second order were specified. As sketched in FIG 1 (b), this resulted in a superposition of an axisymmetric radial offset and a harmonic perturbation of defined amplitude and phase relative to the section camber line. Specifying three parameters at five axial locations means that 15 design parameters were necessary to define the non-axisymmetric contour for one endwall.

2.3 Non-axisymmetric endwall design process

At the time of the study, only very limited information was available about design guidelines for non-axisymmetric endwalls in compressor applications. Additionally, initial parameter studies by hand did not lead to the desired results. Therefore, a semi-automated design process using the Rolls-Royce in-house optimisation tool SOFT was set up in order to quickly and efficiently map the design parameter space and select the most promising parameter sets [10]. A flow diagram of the process is given in FIG 2. First, a database was generated. It was made up of 60 parameter sets that were selected by based on initial parameter studies and configurations that had been read across from turbine applications. Furthermore, 150 additional parameter sets were selected according to $LP-\tau$, a quasi-random design of experiments algorithm [11]. For every parameter set, HYDRA design speed calculations were conducted at three different operating conditions: near choke, at the design point and near stall. The computation time requirement for the numerous HYDRA calculations was reduced by two strategies. Firstly, all three operating conditions were run in parallel for one parameter set. Secondly, by using a well-converged solution from the axisymmetric baseline configuration as initial solution, it became possible to reduce the number of iterations by more than 50 % relative to the nominal case. Overall, this resulted in an evaluation time of approximately two hours for one parameter set, including pre- and postprocessing.

Upon completion of the database, it served as basis to create a response surface model with a linear radial baseline function approach [12]. Subsequently, an optimisation that employed the Adaptive Range Multi-Objective Genetic Algorithm (ARMOGA) was conducted on this response surface [13]. The objectives of the optimisation were to maximise compressor polytropic efficiency and minimise the stator total pressure loss coefficient at all operating points under consideration. No weighting factors were introduced for the different operating points. Constraints included the inlet mass flow rate, compressor total pressure ratio and the stator exit whirl angle. Flow rate and pressure rate were not allowed to assume values lower than the axisymmetric baseline case and the stator exit whirl was not allowed to increase beyond the baseline value. The optimisation consisted of 12 individuals per generation and ran for 1500 generations, yielding a total of 18000 function calls. This high number of evaluations was chosen in order to allow ARMOGA to search a large portion of the design space for a global optimum. However, since the optimisation was conducted on a response surface, the time required for the optimisation still remained small compared to the initial HYDRA CFD calculations. Upon completion of the optimiser run, the resulting parameter set was used to generate a new endwall contour and the geometry was run in HYDRA. The result of this HYDRA calculation was fed back into the database, an updated response surface was generated and another ARMOGA optimisation was conducted on this new response surface. After five to ten updates, the prediction of the response surface lined up reasonably well with the result of the HYDRA calculation and the loop was aborted.

3 COMPRESSOR

This investigation was conducted on a transonic compressor stage. The design reflects a modern

axial high pressure compressor front stage in terms of loading and Mach number levels as well as some key geometrical features such as hub to tip ratio, rotor running clearance etc.

3.1 Baseline configuration

FIG 3. Details of the stator grid domain used for the HYDRA calculations.

The HYDRA setup for the compressor included a stator-rotor-stator arrangement with realistic inlet boundary layer thicknesses. The rotor was modeled including the fillet and a running clearance of 1 % blade height. The stator has no clearance, but a fillet at both hub and casing. Downstream of the stator trailing edge, a portion of the outlet duct was also modeled that had an axial extent of approximately one axial stator chord length. All mesh settings were chosen according to standard values for compressor applications, resulting in approximately 0.5 million cells for each blade row. FIG 3 shows the mesh on the stator blade (black), the hub (blue) and casing (grey) endwalls as well as the periodic boundary (green).
The stator is a 3D refined design in the sense that it satisfies all relevant design criteria from aerodynamic, stress, manufacturing and operational points of view. After reaching an acceptable level of maturity for the stator design, it was equipped with non-axisymmetric endwalls with the process described in section 2.3. The two resulting configurations with and without contoured endwalls are referred to as ”44 stators/contour” and ”44 stators/no contour” in the subsequent sections.

3.2 Configuration with reduced number of stator blades

The stator was the only blade row that was modified during this investigation. The general aerodynamic task of the stator, i.e. the desired radial distribution of stator exit swirl angle, was treated as a constraint in order to ensure comparability between the different configurations.
As a first step, the number of blades was reduced from the baseline design value of 44 to 36, which corresponds to a reduction of approximately 18 %. Next, the camber and thickness distributions, blade inlet and outlet angles as well as chord length of the individual blade sections were modified to account for the changes in blade-to-blade flow field due to the increased space-to-chord ratio. The intention was to reach the same exit whirl angle according to 2D blade-to-blade calculations as the baseline stator with 44 blades while maintaining an acceptable balance between low total pressure losses and high working range. Stress-relevant geometric parameters such as leading and trailing edge radii, the fillet radii at hub and casing as well as maximum section thickness were kept identical to the baseline stator. Also, the axial positions of the leading and trailing edges at hub and casing were not allowed to change. Upon completion of the section design phase, a number of HYDRA calculations were conducted in order to optimise the aerofoil stacking and for final corrections to incidence and deviation.
After no further improvements to the stator flow field could be achieved through ”conventional” 3D aerodynamic design methods, non-axisymmetric endwalls were applied to the new stator by utilising the same semi-automated process as for the baseline stator. The two additional configurations with and without 3D endwalls that resulted from this procedure are referred to as ”36 stators/contour” and ”36 stators/no contour” in the subsequent sections.

4 RESULTS

4.1 Comparison of endwall geometry

The amplitude of the resulting harmonic perturbation reached a maximum level of 1.9 mm, which corresponds to 2.5 % blade height. The maximum observed value of the radial shift was 1.1 mm or 1.5 % blade height. As can be seen in FIG 4 and 5, certain qualitative similarities can be found between the

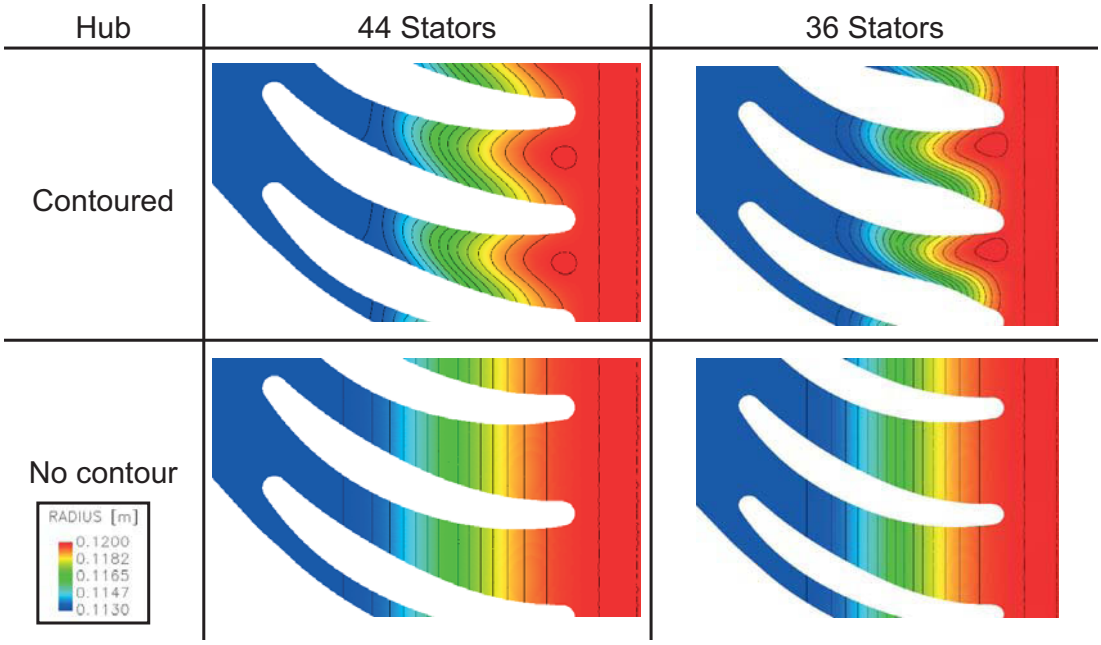

FIG 4. Hub endwall radius contours of the different configurations with and without non-axisymmetric endwalls. White patches indicate the imprints of the blades and the fillets on the hub.

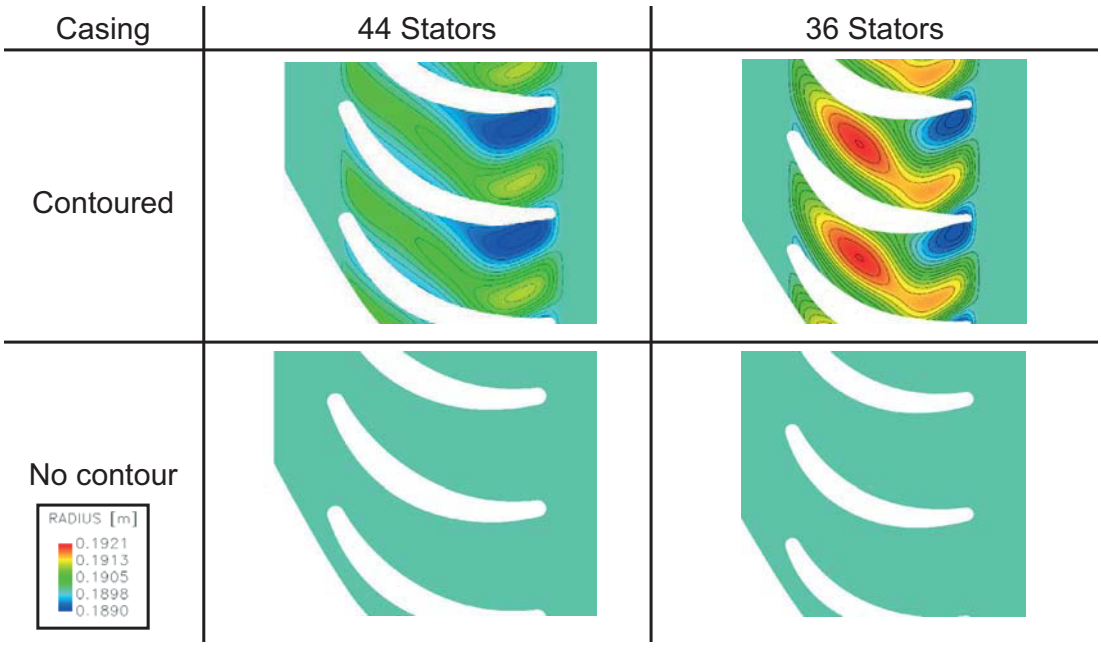

FIG 5. Casing endwall radius contours of the different configurations with and without non-axisymmetric endwalls. White patches indicate the imprints of the blades and the casing fillets on the casing.

endwall contours for the baseline configuration and the one with 36 stators.

At the hub, the harmonic amplitude has very low values of around 0.1 mm at the leading edge and increases towards the trailing edge. The phase shift in the rear half of the blade passage is set to increase the hub radius near the suction side and decrease it close to the pressure side. Near the trailing edge, the circumferential position of the maximum positive radial perturbation lies closer to the suction side for the 36 stators/contour configuration compared to the 44 stators/contour configuration.

The casing contours depicted in FIG 5 show qualitative similarities both between the 44 stators/contour and the 36 stators/contour configurations as well as to the hub contours plotted in FIG 4. In analogy to the hub contours, the amplitude of the harmonic perturbation increases from leading edge to trailing edge. Furthermore, the phase shift near the trailing edge also results in a reduction of flow area close to the suction side and an increase close to the pressure side of the stator. However, the contours at casing also exhibit certain common qualities that are not found at the hub. Near the leading edge, there a visible harmonic perturbation with an amplitude of approximately 0.7 mm. The phase shift in this region is set almost opposite to the one observed near the trailing edge, increasing the flow area near the suction side and decreasing it close to the pressure side. Overall, a ”trench”-like structure can be observed that leads from the leading edge suction side to the trailing edge pressure side of the neighbouring blade. It should be noted that this is opposite to the main direction of the cross-passage secondary flow driven by the static pressure gradient between the suction and pressure sides, which is directed from the leading edge pressure side towards the suction side of the next blade.
The most prominent difference between the casing contours of the 44 stators/contour and the 36 stators/with contour configurations can be observed at approximately 50 % axial chord length. Here, the ”trench” has a depth of around 2 mm for the 36 stators/contour configuration, resulting in a distinctively higher increase in flow area for this configuration.

4.2 Overall performance

FIG 6 shows a comparison of the normalised design speed characteristics of both the 44 and the 36 stator configurations with and without non-axisymmetric endwalls. For the baseline configuration, the impact of the non-axisymmetric endwalls on polytropic efficiency amounts to an increase of 0.05 % at design point conditions. Furthermore, no significant effect on the shape of the pressure ratio versus inlet flow function characteristic or the stability margin of the compressor can be observed.
Without non-axisymmetric endwalls, reducing the number of stator blades from 44 to 36 results in decreased compressor performance. The flow rate is reduced by approximately 0.5 %. The maximum achievable pressure ratio also deceases by 0.5 % relative to the design point pressure ratio. And finally, the polytropic efficiency of the 36 stators/no contour configuration is significantly lower than the 44 stators/no contour configuration throughout the entire characteristic, with a magnitude of 0.9 % at design point conditions.

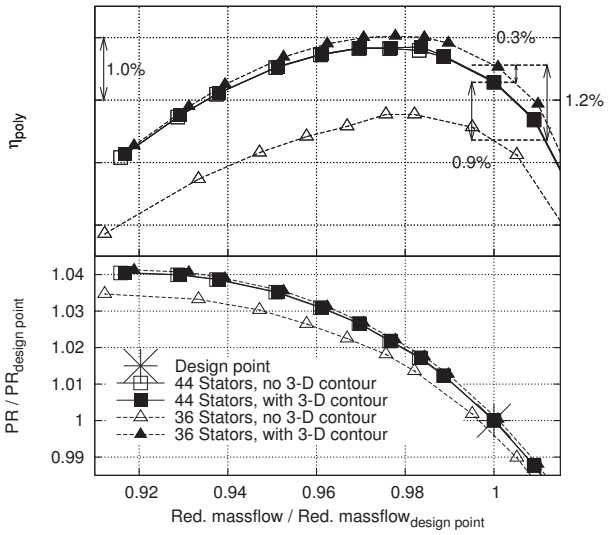

FIG 6. Design speed overall compressor characteristics.

When comparing the characteristics of the 36 stators/no contour and 36 stators/contour configurations, it can be observed that the non-axisymmetric endwalls have a much greater impact on the overall performance of the compressor than was the case with 44 stators. With contouring, the relationship between flow rate and pressure ratio is virtually identical to the baseline case, as is compressor stability. Polytropic efficiency increases across the whole design speed characteristic relative to the 36 stators/no contour configuration, amounting to 1.2 % at design point conditions. At this condition, the 36 stators/contour's efficiency is even 0.3 % above the baseline, making it the configuration with the highest efficiency of all variants considered in this investigation.
Furthermore, the impact of the non-axisymmetric endwalls on the stator exit whirl angle is higher with 36 stators than with 44 stators. While with 44 stators, the average exit whirl improves by approximately 0.25 degrees throughout the whole characteristic, the configuration with 36 stators showed a change in exit whirl of more than 1 degree towards the design intent. Finally, a change in average static pressure ratio can also be observed with 36 stator blades. Without contoured endwalls, the static pressure rise achieved by the blade row decreases across the whole characteristic by an average value of 0.8 % compared to the baseline configuration. When considering the 36 stators/contour variant, no significant difference of the static pressure rise relative to the baseline can be observed.

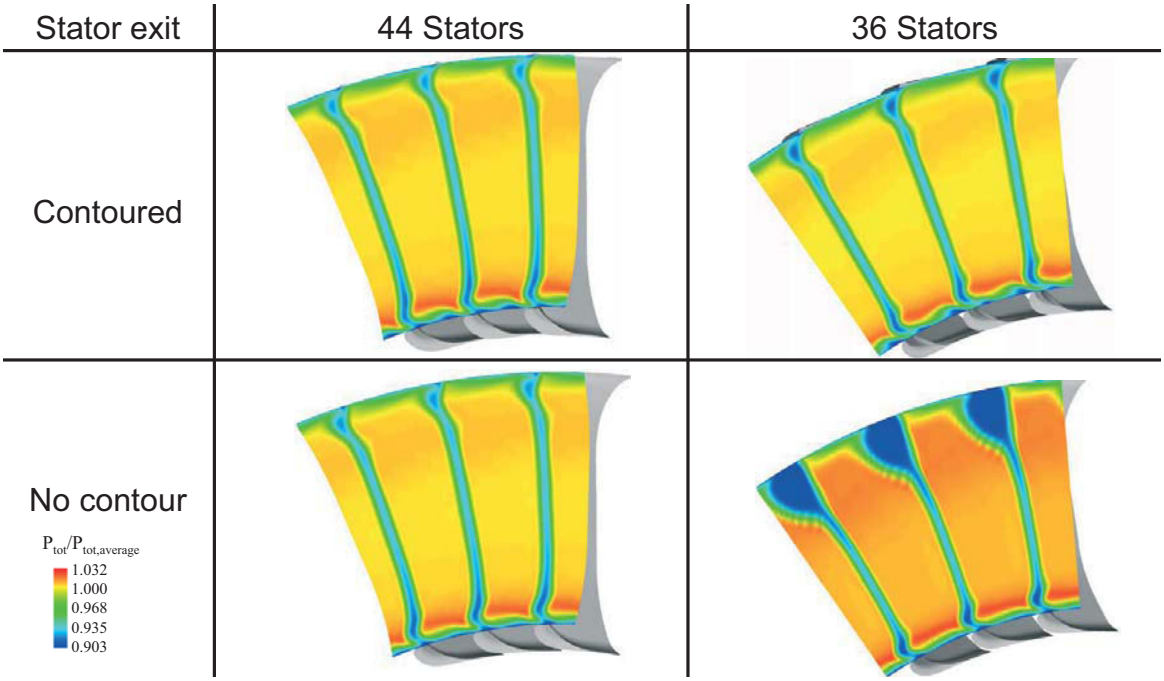

FIG 7. Design point total pressure contours at stator exit for the different configurations with and without non-axisymmetric endwalls.

4.3 Design point performance

In order to better understand the mechanisms that lead to the observed differences in impact of the non-axisymmetric contours on compressor overall performance, a more detailed analysis of the stator flow field at design point conditions was conducted. Contour plots of normalised total pressure in an axial plane at stator exit are shown in FIG 7. With 44 stators, the qualitative appearance of the pressure distribution does not differ significantly between the variants with and without non-axisymmetric endwalls. The wakes of the stator trailing edges are visible as low pressure zones with small circumferential extent. Close to the hub and casing, the circumferential extent of these low pressure zones increases, most likely as a result of the influence of the secondary flows. In contrast to this, a low pressure area that extends approximately one third of the duct height in radial direction and half of one blade pitch circumferentially, can be observed near the casing for the 36 stators/no contour configuration. With contoured endwalls, this pronounced low pressure zone disappears, resulting in a pressure distribution for the 36 stators/contour variant that qualitatively resembles the cases with 44 stators.

Radial distributions of circumferentially averaged stator total pressure loss coefficient in FIG 8 show that the low pressure zone in FIG 7 corresponds to an area of high loss for the 36 stators/no contour variant. With contoured endwalls, the amount of loss generated near the casing is reduced to the level of the variants with 44 stators. This corresponds to a reduction in average loss coefficient of approximately 30 % for the 36 stators variant which can be accounted to the presence of the non-axisymmetric endwalls. In addition, it should be noted that between 10 % and 90 % annulus height, the 36 stators/contour configuration reaches a lower loss level relative to the 44 stator configurations. Since the losses of IGV and ro-

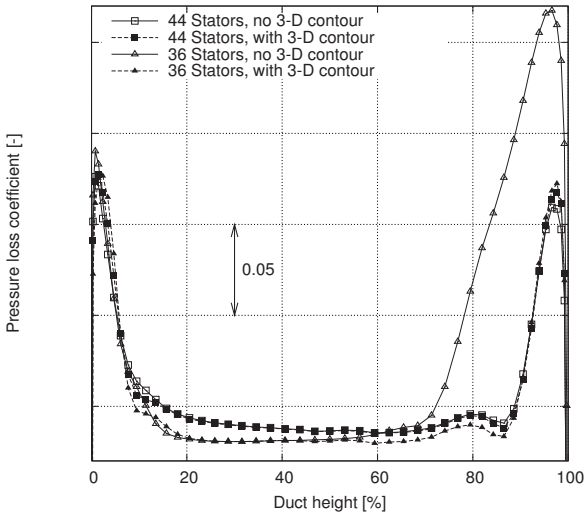

FIG 8. Design point radial distributions of total pressure loss coefficient.

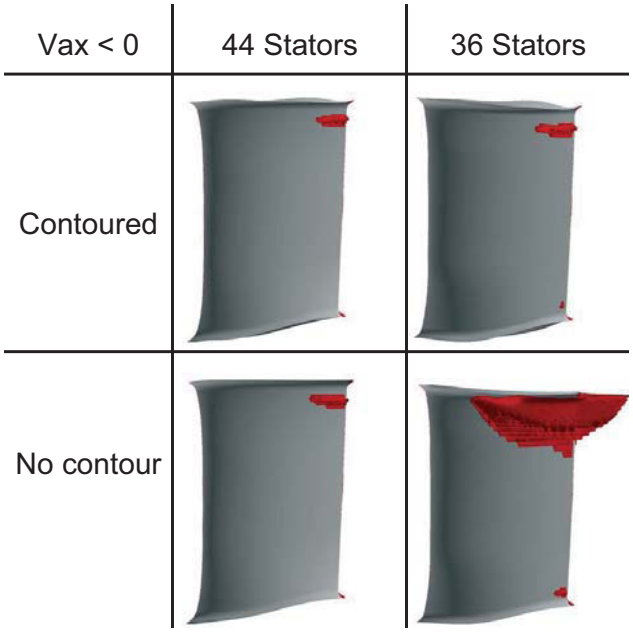

FIG 9. Iso-surface of design point reverse flow areas for the different configurations.

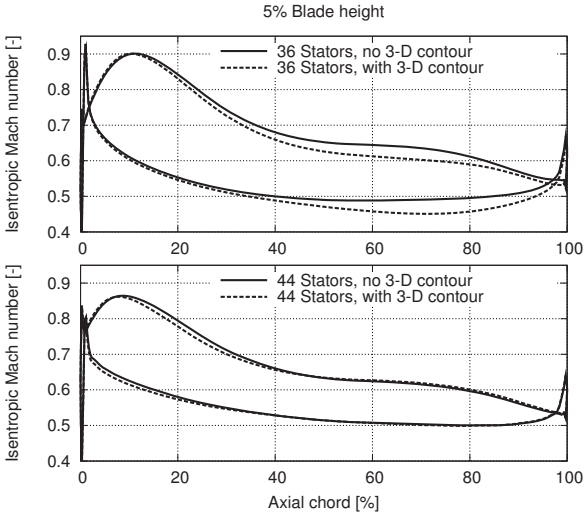

FIG 10. Distributions of aerofoil surface isentropic Mach number at 5 % blade height.

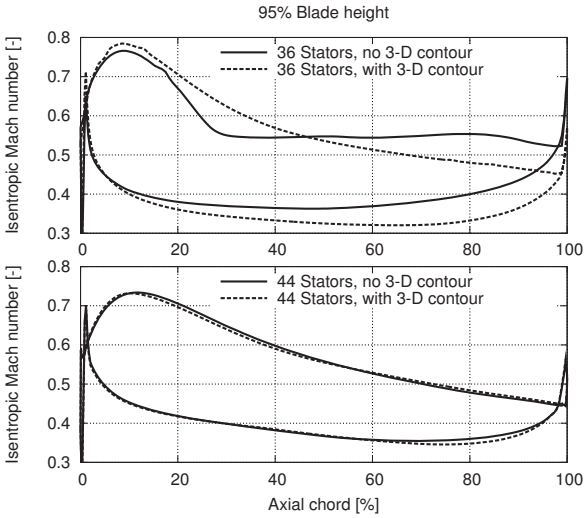

FIG 11. Distributions of aerofoil surface isentropic Mach number at 95 % blade height.

tor did not change for any of the four configurations, the combination of comparable near-wall losses and lower main flow losses is interpreted as the reason why the 36 stators/contour configuration shows the highest design point efficiency of all variants considered in this study.

A survey of the areas with reverse flow was conducted by plotting iso-surfaces of negative axial velocity. A comparison of the resulting iso-surfaces is given in FIG 9. It can be seen that the 36 stators/no contour configuration has the biggest reverse flow zone close to the casing, corresponding to the area of high total pressure loss in FIG 8. Application of non-axisymmetric endwalls indicates a reduction of this reverse flow zone back to the extend visible for both 44 stators configurations. Therefore, it is concluded that the main mechanism of loss reduction exploited by the non-axisymmetric endwalls in the present study is the suppression of stator casing corner stall. This is also supported by the observation that the near-casing reverse flow region is of significantly smaller size for the 44 stators/no contour variant than for the 36 stators/contour configuration, thus leaving a greatly reduced improvement potential to be exploited by application of contoured endwalls.

Distributions of blade surface isentropic Mach number close to the stator hub and casing are given in FIG 10 and FIG 11, respectively. It becomes clear that the non-axisymmetric endwalls cause a redistribution of the local blade loading. At the hub, a shift of the suction side peak Mach number towards the leading edge can be observed for both 44 and 36 stators. The value of the peak Mach number remains constant. The deceleration of the flow and corresponding static pressure rise, visible as a decrease in suction side Mach number, is accomplished more rapidly and in the case of 36 stators, also leads to lower levels at the trailing edge. Overall, the load is lowered in the mid-chord area and increased near the leading and trailing edge. At the casing, FIG 11 shows that a qualitatively similar change in Mach number distribution takes place for the 44 stators configuration. However, both qualitative and quantitative changes are observed with 36

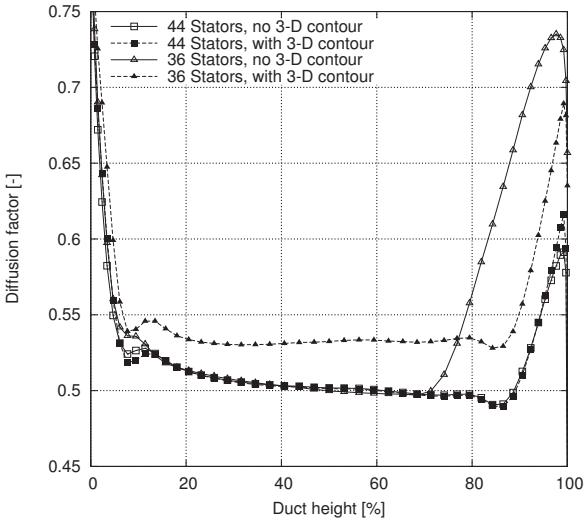

FIG 12. Radial distributions of stator diffusion factor.

stators. Without endwall contouring, the suction side Mach number stays almost constant from approximately 30 % axial chord length. This indicates a separation of the blade suction surface boundary layer and the subsequent formation of a blockage area in the flow path, thus preventing any further deceleration of the flow. With contour, this deceleration is now accomplished by suppressing separation and decreasing blockage in the blade passage, resulting in the altered suction surface Mach number distribtion.

Radial distributions of circumferentially averaged diffusion factor are plotted in FIG 12. The diffusion factor DF was derived according to

$$DF = (1 - \frac{V_2}{V_1}) + \frac{\Delta V_\theta}{2\sigma V_1} \quad (1)$$

where $V_1$is the stator inlet total velocity, V_2 is the stator exit total velocity, ΔV_θ is the difference in circumferential velocity across the blade row and σ is the solidity, e.g. the ratio of chord length to blade spacing.

The figure demonstrates how the design parameter space, in this case the feasible range of stator blade numbers, was extended by the possibility to apply non-axisymmetric endwalls to the stator. For the baseline design, the number of stator blades was set to reach a limiting diffusion factor of about 0.50 at blade mid height in order to enable acceptable stator performance at the given aerodynamic environment. Decreasing the solidity by reducing the number of blades increases the diffusion factor even more. Without non-axisymmetric endwalls, this leads to massive changes in the flow field and as a consequence, a significantly altered radial distribution of diffusion factor. Close to the casing, where the large separation zone described earlier is located, the diagram shows a disproportionate increase in local aerodynamic loading as a result of the low stator exit velocity. While the high blockage near the casing leads to a higher level of inlet velocity between about 10 % and 70 % of the blade height and therefore lower loading, it becomes clear that overall, reducing the number of blades without non-axisymmetric endwalls increases the loading beyond levels that are manageable by 3D blade design methods alone. The highest level of diffusion factor seen in FIG 12 only results in an acceptable design once non-axisymmetric endwall contours are introduced. Thus, it can be concluded that non-axisymmetric endwalls allow the aerodynamic designer to extend the range of diffusion factor where blades can still operate with satisfying performance.

5 CONCLUSIONS

It was demonstrated that application of non-axisymmetric endwall contouring to the endwalls of a highly loaded stator only leads to significant improvements in aerodynamic performance if a separation zone of significant size is present in the configuration without contour. Therefore, suppression of near-wall separation zones is identified as the main flow feature that can be controlled by this technology. Furthermore, it was demonstrated how the non-axisymmetric endwalls can be used as a means of extending the design parameter space beyond the range that is accessible by conventional 3D design methods alone. The possibility to reduce the number of stator blades while maintaining or increasing design speed efficiency would also lead to further benefits in terms of weight and cost savings.

Further studies should include a more detailed analysis of the stall-suppressing mechanism of the endwall contours as well as alternative ways of using this technology to improve the aerodynamic properties in a high-pressure compressor environment. Finally, experimental validation of the findings of this numerical study would help to understand the true potential that non-axisymmetric endwall contours offer.

6 ACKNOWLEDGMENT

The work presented in this paper was carried out under the framework of the research programme *Verdichterdesign und -modellierung für Vision 10 Triebwerkskonzepte (VerDeMod)* with funding from the German Federal Government, funding reference number 20T0609. The authors would also like to thank Rolls-Royce Deutschland Ltd & Co KG for the

permission to publish this paper.

REFERENCES

[1] V. Iliopoulou, I. Lepot, and P. Geuzaine. Design optimization of a hp compressor blade and its hub endwall. *Proceedings of ASME Turbo Expo*, (GT-2008-50293), 2008.

[2] M. Hoeger, N. Sievers, and M. Lawerenz. On the performance of compressore blades with contoured endwalls. *Euroturbo 4*, (ATI-CST-060/01), 2001.

[3] M. Hoeger, P. Cardamone, and L. Fottner. Influence of endwall conturing on the transonic flow in a compressor blade. *Proceedings of ASME Turbo Expo*, (GT-2002-30440), 2002.

[4] E. M. J. Naylor, C. O. Duenas, R. J. Miller, and H. P. Hodson. Optimisation of non-axisymmetric endwalls in compressor s-shaped ducts. *Proceedings of ASME Turbo Expo*, (GT-2008-50448), 2008.

[5] S. Reising, H.-P. Schiffer, T. Hildebrandt, and P. Thiel. Automated aerodynamic optimisation of a transonic compressor stage by application of non-axisymmetric endwalls. *DGLR Jahrestagung*, 2008.

[6] C. Dorfner, E. Nicke, and C. Voss. Axis-asymmetric profiled endwall design using multiobjective optimization linked with 3d rans-flow simulations. *Proceedings of ASME Turbo Expo*, (GT-2007-27268), 2007.

[7] N. Harvey. Some effects of non-axisymmetric end wall profiling on axial flow compressor aerodynamics. part i: Linear cascade investigation. *Proceedings of ASME Turbo Expo*, (GT-2008-50990), 2008.

[8] N. Harvey and T. Offord. Some effects of non-axisymmetric end wall profiling on axial flow compressor aerodynamics. part ii: Multi-stage hpc cfd study. *Proceedings of ASME Turbo Expo*, (GT-2008-50991), 2008.

[9] S. Shahpar and L. Lapworth. Padram: Parametric design and rapid meshing system for turbomachinery optimisation. *Proceedings of ASME Turbo Expo*, (GT-2003-38698), 2003.

[10] S. Shahpar. Soft: A new design and optimisation tool for turbomachinery. *Evolutionary Methods for Design, Optimisation and Control*, 2002.

[11] I. M. Sobol. On the systematic search in a hypercube. *SIAM Journal of Numerical Analysis*, 16, 1979.

[12] M. D. Buhmann. *Radial Basis Functions: Theory and Implementations*. Cambridge University Press, 2003.

[13] D. Sasaki and S. Obayashi. Low-boom design optimization for sst canard-wing-fuselage configuration. *AIAA Computational Fluid Dynamics Conference*, (AIAA-2003-3432), 2003.